

# Exploiting Test-Time Augmentation in Federated Learning for Brain Tumor MRI Classification

Thamara Leandra de Deus Melo<sup>1</sup>, Rodrigo Moreira<sup>1</sup> <sup>a</sup>,  
 Larissa Ferreira Rodrigues Moreira<sup>1</sup>  <sup>b</sup>, André R. Backes<sup>2</sup>  <sup>c</sup>

<sup>1</sup>*Institute of Exact and Technological Sciences, Federal University of Viçosa - UFV, Rio Paranaíba-MG, Brazil*

<sup>2</sup>*Department of Computing, Federal University of São Carlos, São Carlos-SP, Brazil*  
 {thamara.melo, rodrigo, larissa.f.rodrigues}@ufv.br; arbackes@yahoo.com.br

**Keywords:** Brain tumors, Federated Learning, Test-Time Augmentation, Image classification

**Abstract:** Efficient brain tumor diagnosis is crucial for early treatment; however, it is challenging because of lesion variability and image complexity. We evaluated convolutional neural networks (CNNs) in a federated learning (FL) setting, comparing models trained on original versus preprocessed MRI images (resizing, grayscale conversion, normalization, filtering, and histogram equalization). Preprocessing alone yielded negligible gains; combined with test-time augmentation (TTA), it delivered consistent, statistically significant improvements in federated MRI classification ( $p < 0.001$ ). In practice, TTA should be the default inference strategy in FL-based medical imaging; when the computational budget permits, pairing TTA with light preprocessing provides additional reliable gains.

## 1 INTRODUCTION

Brain tumors are among the most aggressive neurological disorders with high morbidity and mortality. Diagnosis is difficult because lesions exhibit heterogeneous morphologies, variable intensity profiles, and complex appearances on Magnetic Resonance Imaging (MRI) (Stupp et al., 2005; Louis et al., 2021; Carmo et al., 2025). Although MRI is the gold standard for noninvasive assessment, interpretation depends on specialist expertise, which introduces variability and limits scalability in routine clinical practice (Wen and Butler, 2020).

Recent advances in Artificial Intelligence (AI), particularly in Convolutional Neural Network (CNN)-based models, have improved automated tumor assessment by learning discriminative features directly from images (Goodfellow et al., 2016; Rodrigues et al., 2017; Rodrigues Moreira et al., 2025). However, privacy regulations and institutional policies often preclude centralizing of patient data across hospitals. Federated Learning (FL) addresses this barrier by training shared models locally at each site without exposing raw data, promoting generalization across

heterogeneous cohorts while preserving confidentiality (McMahan et al., 2017; Konečný et al., 2016; Rodrigues et al., 2025).

Despite the growing use of FL in medical imaging, the impact of common preprocessing pipelines on federated performance for brain tumor MRI classification remains unclear. Standard operations (e.g., resizing, grayscale conversion, normalization, filtering, and histogram equalization) may harmonize inputs across clients; however, they can also suppress subtle, clinically relevant cues. At the same time, the potential of Test Time Augmentation (TTA) at inference, known to reduce prediction variance in centralized settings, has not been examined under federated conditions, where client heterogeneity (scanners, protocols, and demographics) is the norm (Wang et al., 2019; Islam et al., 2024).

TTA is model-agnostic, requires no retraining, and can be deployed unilaterally at inference time by each client, all of which are attractive properties in FL where retraining is costly, communication budgets are tight, and data cannot be pooled. If effective, TTA offers a low-overhead mechanism to improve robustness and stabilize predictions against interclient distribution shifts and small-sample effects without modifying the federated optimization process.

Guided by the gaps identified, we raise the following research questions (RQs) to structure our investi-

<sup>a</sup> <https://orcid.org/0000-0002-9328-8618>

<sup>b</sup> <https://orcid.org/0000-0001-8947-9182>

<sup>c</sup> <https://orcid.org/0000-0002-7486-4253>

gation:

- **RQ1:** Does preprocessing help or hinder brain-tumor classification in FL when compared with training on original (minimally processed) MRI images?
- **RQ2:** To what extent does TTA improve prediction robustness and accuracy during federated inference across heterogeneous clients?

This study addresses these gaps by proposing an FL framework for brain tumor MRI classification that compares original and preprocessed images and integrates TTA during inference. Our contributions are as follows: (i) we evaluate the influence of preprocessing pipelines on federated performance, (ii) we exploit TTA to enhance prediction stability and accuracy, and (iii) quantify effects via statistical hypothesis testing.

Our results show that preserving native MRI characteristics yields better federated performance than aggressively preprocessed inputs and that TTA provides a consistent, low-cost robustness boost. These findings provide practical data-retentive design choices for decentralized medical AI systems.

The remainder of this paper is organized as follows. Section 2 reviews related work. Section 3 describes the proposed method, including the MRI dataset, preprocessing pipeline, federated setup, and integration of TTA. Section 4 presents and discuss the experimental results. Finally, Section 5 concludes the paper and outlines future research directions.

## 2 RELATED WORK

The detection and classification of brain tumors in MRI images has been the subject of extensive investigation, given the severity of this condition and the need for early and accurate diagnoses. Machine learning and deep learning techniques have been prominently applied in this context, especially Convolutional Neural Networks (CNNs), which have proven efficient in extracting discriminative patterns in medical images Solanki et al. (2023); Siddique et al. (2022).

Shah et al. (2022) presented a model based on the EfficientNet-B0 architecture for brain tumor classification, combined with *fine-tuning* techniques and data augmentation. The authors compared the model with traditional architectures such as VGG16, InceptionV3, Xception, ResNet50, and InceptionResNetV2. The proposed model outperformed all baselines, achieving an accuracy of 98.87% and an AUC of 0.988.

Khaliki and Başarslan (2024) compared the performance of conventional CNNs and pretrained models such as VGG19, EfficientNetB4, and InceptionV3 on Kaggle dataset images. The results demonstrated that the use of *transfer learning* significantly improves classification, particularly in scenarios with limited datasets.

Kaur and Mahajan (2025) explored the use of ResNet152 and GoogleNet for feature extraction, combined with traditional classifiers such as SVM, KNN, CART, and GNB. The pipeline also included preprocessing, PCA, and data augmentation. The study achieved an accuracy of 98.53% and an F1-score of 97.4%, highlighting the relevance of image preparation and architectural choice for consistent results.

In the field of FL, Zhou et al. (2024) demonstrated the feasibility of decentralized training across multiple medical institutions using the BRATS dataset. The study evaluated several CNNs, including ResNet50, VGG16, EfficientNet, and AlexNet, achieving accuracy above 95%. Similarly, Albalawi et al. (2024) integrated FL and *transfer learning* with a modified VGG16, obtaining 98% accuracy and an F1-score above 0.95 while preserving the privacy of sensitive data.

Thus, the literature highlights significant advances in brain tumor classification in both centralized and distributed scenarios. Unlike the aforementioned works, this study focuses on comparing original and preprocessed images in a FL environment, using ResNet18 to evaluate the impact of preprocessing on classification performance.

Table 1 summarizes the main characteristics of the mentioned studies on brain tumor MRI classification. To improve readability, the table uses a checklist notation:  $\checkmark$  indicates that the feature or technique was explicitly employed in the study, whereas  $\times$  indicates its absence. This compact format allows direct comparison of datasets, model backbones, preprocessing, FL usage, and evaluation metrics.

Unlike previous studies, this study advances the field by comparing original and preprocessed MRI images in a federated setting, revealing that preserving the raw image structure can yield superior performance. We are among the first to exploit TTA within FL for brain-tumor classification, demonstrating its role in improving prediction stability and highlighting the differences between data preparation strategies. We reinforce our findings with rigorous statistical hypothesis testing, providing quantitative evidence of effect size and significance, which is often overlooked in related studies.

Table 1: Comparison with related work.

Work	Dataset	Method	Pre/Aug.	FL	Metrics
Shah et al. (2022)	BRATS 2015	EfficientNet-B0	✓	✗	Acc, AUC
Jiang et al. (2022)	BRATS 2019–21	3D Swin Transformer	✓	✗	Dice, HD
Khaliki and Başarslan (2024)	Kaggle (MRI)	VGG19, EfficientNetB4, InceptionV3	✓	✗	Acc, F1, AUC
Shaikh et al. (2025)	BRATS 2020–23	Ensemble of CNNs	✓	✗	Acc, F1, Dice
Kaur and Mahajan (2025)	Br35 (Kaggle)	ResNet152, GoogleNet	✓	✗	Acc, F1
Zhou et al. (2024)	BRATS 2015–18	ResNet50, VGG, EffNet	✗	✓	Acc, F1, AUC
Albalawi et al. (2024)	Figshare, Br35H	VGG16 + FL (10 clients)	✓	✓	Acc, F1
<b>Ours</b>	<b>Kaggle MRI</b>	<b>ResNet18 + TTA</b>	<b>✓</b>	<b>✓</b>	<b>Acc, F1, Recall, Precision</b>

### 3 MATERIAL AND METHODS

We investigated how input preprocessing and test-time augmentation (TTA) affect brain–tumor MRI classification under federated learning (FL). Figure 1 shows an end-to-end workflow.

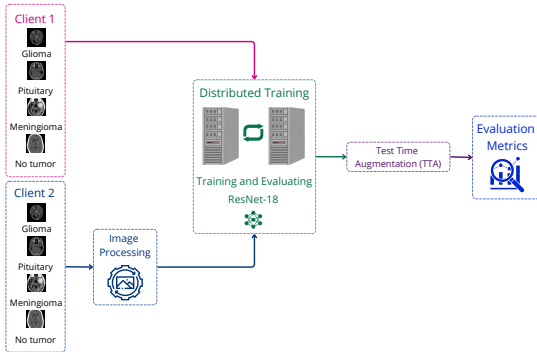


Figure 1: Proposed Method.

Two clients participated in FL: Client 1 received the original (minimally processed) images, whereas Client 2 consumed the preprocessed images produced by a standard preprocessing pipeline. Each client trains a local ResNet-18 on its private subset; after each communication round  $r$ , local parameters  $w_i^{(r)}$  are sent to the server, which aggregates them via FedAvg to obtain the global model  $w^{(r+1)}$ .

Once training converges, inference is performed with TTA. For each test image,  $K$  stochastic views are generated, scored by the global model, and combined (e.g., by averaging) into a final prediction.

#### 3.1 Image Dataset

We use the public Brain MRI dataset from Kaggle<sup>1</sup>, a widely adopted in the literature for brain-tumor classification. The dataset consists of 2D axial brain MRI slices, provided as raster images with variable spatial resolutions and aspect ratios.

The images were labeled into four categories: no tumor, glioma, meningioma, and pituitary. In the original release, the class counts are no tumor (2000), glioma (1621), meningioma (1645), and pituitary (1757), totaling 7023 images. Table 2 presents the distribution of instances per class along with representative visual examples.

Table 2: Class distribution with visual examples.

Class	Quantity	Example
No Tumor	2000	
Glioma	1621	
Meningioma	1645	
Pituitary	1757	
<b>Total</b>	<b>7023</b>	

<sup>1</sup><https://www.kaggle.com/datasets/masoudnickparvar/brain-tumor-mri-dataset>

To mitigate information leakage and prevent optimistic bias, we removed duplicate data prior to splitting the dataset. We identified exact bit-for-bit duplicates by calculating the SHA-256 hash for each file, finding all byte-identical matches regardless of their class. A total of 194 duplicate images were removed, resulting in a final working dataset of 6,829 unique images for all experiments (National Institute of Standards and Technology, 2012).

## 3.2 ResNet-18 Backbone

We adopted ResNet-18 as the convolutional backbone for all experiments. ResNet implements residual learning and instead of learning direct mapping  $H(x)$ , each block learns a residual function  $F(x) = H(x) - x$  and reintroduces the input through an identity shortcut  $x + F(x)$ . This design facilitates optimization in deeper models by preserving the gradient flow and mitigating the vanishing gradients (He et al., 2016).

ResNet-18 comprises four stages of basic blocks with  $3 \times 3$  convolutions, each followed by batch normalization and ReLU. Downsampling was performed using stride 2 in the first block of each stage. The channel widths per stage were [64, 128, 256, 512] with block counts [2, 2, 2, 2]. A  $7 \times 7$  convolution and max pooling form the stem, and the network ends with global average pooling and a fully connected classifier (Fig.2).

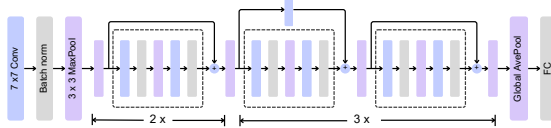


Figure 2: Schematic of the ResNet 18 architecture with basic residual blocks and four stages of increasing channel width.

This CNN has approximately 11.7 M parameters, which offers a favorable balance between the representational capacity and communication cost in FL rounds (Rodrigues Moreira et al., 2025). Local updates are computed for each client, and the resulting parameters are aggregated by FedAvg on the server. ResNet-18 is sufficiently compact for fast rounds in FL. When the hardware allows, we use 16-bit (FP16) weights, which take approximately half the memory and bandwidth of 32-bit (FP32) to further speed up communication without changing the architecture. This keeps both the original and preprocessed pipelines directly comparable.

## 3.3 Federated Learning

Federated Learning (FL) is a decentralized training paradigm in which data never leave the client devices (e.g., hospitals); only model updates are transmitted to a coordinating server that computes a global model (McMahan et al., 2017). This design aligns with medical privacy requirements by avoiding the centralization of sensitive MRI data, while still enabling collaborative learning across institutions (Konečný et al., 2016; Rodrigues et al., 2025).

Training proceeds in synchronous communication rounds  $r \in \{0, \dots, R-1\}$ . At the start of round  $r$ , the server broadcasts the current global parameters  $\mathbf{w}^{(r)}$  to the participating clients  $\mathcal{C}_r$ . Each client  $i \in \mathcal{C}_r$  performs local training and returns  $\mathbf{w}_i^{(r)}$ . The server updates the global model via sample-size-weighted averaging (Equation 1).

$$\mathbf{w}^{(r+1)} = \frac{\sum_{i \in \mathcal{C}_r} n_i \mathbf{w}_i^{(r)}}{\sum_{j \in \mathcal{C}_r} n_j}. \quad (1)$$

Where  $n_i$  denotes the number of training samples held by client  $i$ , and  $\mathcal{C}_r$  is the set of clients participating in round  $r$ . Figure 3 depicts the standard FL topology with clients and servers.

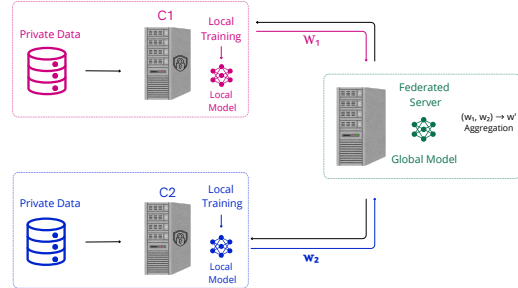


Figure 3: Basic FL topology.

Medical datasets are typically fragmented across sites, collected using heterogeneous scanners and protocols, and cannot be pooled because of consent and regulatory constraints. FL leverages this diversity without moving raw data, improving generalization while preserving confidentiality. Moreover, Federated Averaging (FedAvg) is communication efficient and robust under non-IID partitions, making it a practical baseline for clinical deployment (Barbosa et al., 2025; Rodrigues et al., 2025).

### 3.4 Image Preprocessing

We describe the input pipelines used before training and inference. The goals are: (i) harmonize files of varying size and color encoding so they are compatible with a pretrained ResNet-18 backbone, and (ii) in the preprocessed strategy, test whether standard intensity/denoising operations help or hinder performance in our federated setup.

#### Original (minimal processing)

- **Resize:** rescale each image to  $224 \times 224$ .
- **Channels:** if single-channel, replicate to three channels (for ImageNet initialization).
- **Normalization:** apply the same ImageNet mean and standard deviation normalization.
- **No intensity shaping:** no denoising, no histogram equalization, and no remapping beyond the normalization above.

#### Preprocessed (harmonization pipeline)

- **Grayscale standardization:** convert to single-channel and replicate to three channels.
- **Resize:** rescale each image to  $224 \times 224$ .
- **Pixel normalization:** scale raw intensities to  $[0, 1]$ .
- **Light denoising:** apply a mild noise-reduction filter (e.g., small-kernel median or Gaussian).
- **Histogram equalization:** global equalization to broaden dynamic range in low-contrast slices.
- **Normalization:** apply the same ImageNet mean and standard deviation normalization.

### 3.5 Test Time Augmentation

Test Time Augmentation (TTA) consists of applying data augmentation techniques during the inference phase rather than exclusively during training (Mari et al., 2025). Let  $x$  denote an input image and  $\mathcal{T} = \{T_1, T_2, \dots, T_K\}$  the set of stochastic transformations applied to  $x$  (e.g., rotations, flips, or intensity adjustments). For each transformation  $T_k$ , the model  $f_\theta$  produces a prediction as expressed in Equation (2):

$$\hat{y}_k = f_\theta(T_k(x)), \quad k = 1, \dots, K. \quad (2)$$

The final prediction  $\hat{y}$  is then obtained by aggregating the  $K$  outputs. For probabilistic outputs, the arithmetic mean is typically employed, as shown in Equation (3):

$$\hat{y} = \frac{1}{K} \sum_{k=1}^K \hat{y}_k, \quad (3)$$

whereas for categorical predictions, majority voting is often used, as in Eq. (4):

$$\hat{y} = \arg \max_c \sum_{k=1}^K 1\{\hat{y}_k = c\}, \quad (4)$$

where  $c$  indexes the possible classes and  $1\{\cdot\}$  is the indicator function.

Prior work has grounded TTA both theoretically and empirically in medical imaging. (Wang et al., 2019) formalized TTA for tumor segmentation, showing gains over conventional inference and providing more reliable uncertainty estimates. (Islam et al., 2024) further positioned TTA as strategy of modern augmentation pipelines, highlighting improvements in generalization. Building on these insights, we deploy TTA in a federated classification setting to probe its effect on the accuracy and stability under client heterogeneity. Our use is model-agnostic and retraining-free: multiple stochastic views are aggregated at inference, and we compare the outcomes for models trained on original versus preprocessed MRI inputs.

Figure 4 illustrates the practical application of TTA to an original MRI sample. From a single input image, the process generates multiple stochastic views featuring transformations. These modifications maintain the anatomical integrity of the tumor region while introducing sufficient diversity to evaluate the model’s robustness against realistic input variations. We fix the augmentation budget to  $K=10$  stochastic views per test image in our experiments.

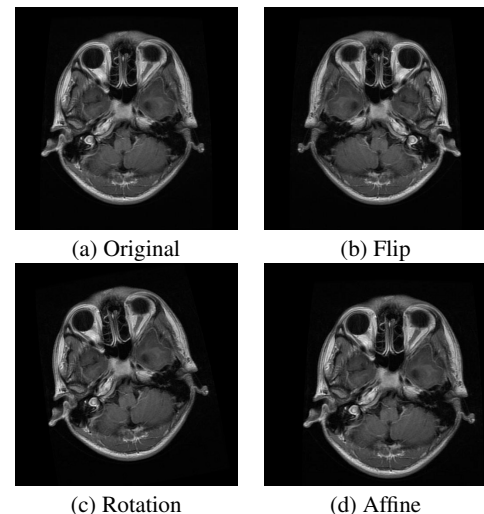


Figure 4: Original MRI scan and TTA-generated variations.

### 3.6 Evaluation Metrics

We evaluate performance with standard classification metrics: Accuracy, Precision, Recall, and F1-Score (Solanki et al., 2023). Let  $TP$  (true positives),  $TN$  (true negatives),  $FP$  (false positives), and  $FN$  (false negatives) denote the entries of the confusion matrix.

- **Accuracy:**

$$Acc = \frac{TP + TN}{TP + TN + FP + FN}$$

Measures the proportion of correctly classified instances relative to the total number of samples.

- **Precision:**

$$Prec = \frac{TP}{TP + FP}$$

Evaluates the proportion of positive predictions that are actually correct.

- **Recall:**

$$Recall = \frac{TP}{TP + FN}$$

Measures the model’s ability to correctly identify positive cases.

- **F1-Score:**

$$F1 = 2 \cdot \frac{Precision \cdot Recall}{Precision + Recall}$$

Represents the harmonic mean between Precision and Recall, particularly useful in scenarios with imbalanced classes.

## 4 RESULTS AND DISCUSSION

All experiments were performed on a workstation with an Intel(R) Core(TM) i5-8400 CPU @ 2.80 GHz, 16 GB RAM, and an NVIDIA GeForce RTX 2060 SUPER GPU. We used Python 3.8.10, PyTorch 2.4.1, and the Flower FL framework 1.11.1 (Beutel et al., 2020).

We first removed the exact duplicate images using the SHA-256 cryptographic hash. After deduplication, we created stratified train/test partitions (80/20) to preserve the class proportions observed in the full dataset in each split. For the federated setup, stratified subsets were assigned to each client, ensuring that (i) no image appeared in more than one split or client and (ii) both clients held representative samples from all classes. Because patient- or series-level metadata are unavailable, stratification was performed at the image level.

Both input strategies, Original and Preprocessed, operate on the same splits. In the Original strategy,

images are consumed as provided (file decoding and tensor conversion only). In the Preprocessed strategy, we applied a harmonization pipeline prior to training.

For  $K > 1$  augmented views, each test image is stochastically transformed using: resizing to  $224 \times 224$ , random horizontal flip ( $p = 0.5$ ), random rotation ( $\pm 10^\circ$ ,  $p = 0.5$ ), and a small random affine (translation  $\leq 5\%$ , scale  $[0.95, 1.05]$ ,  $p = 0.5$ ), followed by normalization. Predictions from the  $K$  views are aggregated by averaging the class probabilities or by majority voting. When  $K = 1$ , we apply only deterministic resizing and normalization. All preprocessing steps are deterministic within each strategy; the only stochasticity arises from TTA at inference. Both federated clients used identically configured pipelines within their assigned strategies (Original vs. Preprocessed).

We trained for three communication rounds, with 50 local epochs per round and mini-batches of size 32. Optimization used Adam (learning rate 0.001); aggregation used standard FedAvg. In each round, both clients participated ( $|\mathcal{C}_r| = 2$ ; client fraction = 1.0). We evaluated both the Original and Preprocessed input strategies with and without TTA, reporting descriptive metrics and paired statistical tests to assess the significance of performance differences across clients.

### 4.1 Federated Baseline without TTA

We established a baseline by isolating the training-time processing without inference-time ensembling. The global model leads across all metrics, indicating that parameter aggregation via FedAvg yielded a stronger classifier than either client. Figure 5 shows the baseline performance of the global model and both clients without TTA and the global model surpasses either client across metrics.

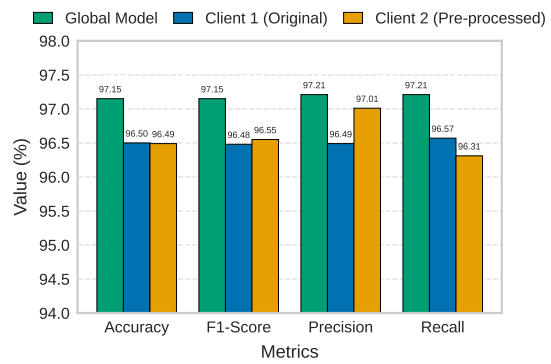


Figure 5: Performance metrics without TTA.

The two clients produced comparable results; a small advantage appeared for the client trained on the original images (96.50% accuracy) over the pre-processed client (96.49%). Aggregation does more than smooth noise: it combines complementary error patterns to improve discrimination (Precision/F1) and coverage (recall). Effect sizes remain small, suggesting that per-client models are already strong under this dataset and partitioning, and that input processing choices primarily fine-tune calibration and operating points rather than driving large swings in accuracy.

## 4.2 Effect of TTA

The introduction of TTA clarified the performance gap between the strategies. Figure 6 contrasts Client 1 (Original) and Client 2 (Preprocessed) with TTA; the chart aligns with Table 3.

With TTA, the preprocessed client shows slightly superior performance (e.g.,  $\approx 0.4 - 0.5$  percentage points), a modest but consistent margin that reflects gains in stability and precision from combining input standardization with augmented inference. This advantage likely stems from reduced noise and standardized inputs, which make predictions less sensitive to spatial and contrast variations. Concurrently, TTA stabilizes the predictions and exposes small but systematic differences between the training configurations.

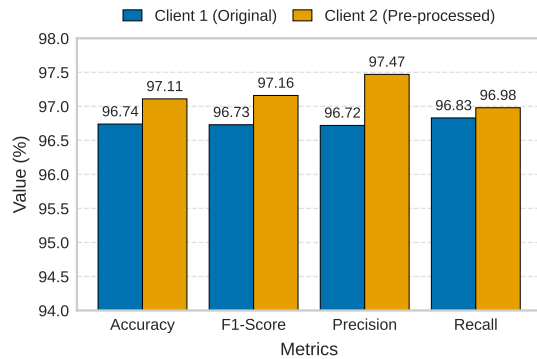


Figure 6: Performance comparison using TTA.

Table 3: Results obtained with TTA (10 runs). Client 1 (original) and Client 2 (preprocessed).

C	Acc. (%)	F1 (%)	Prec. (%)	Rec. (%)
1	96.74	96.73	96.72	96.83
	$\pm 0.15$	$\pm 0.15$	$\pm 0.15$	$\pm 0.14$
2	<b>97.11</b>	<b>97.16</b>	<b>97.47</b>	<b>96.98</b>
	$\pm 0.19$	$\pm 0.18$	$\pm 0.16$	$\pm 0.20$

## 4.3 Statistical Analysis

We evaluate whether preprocessing improves performance under a fixed test-time augmentation budget (TTA with  $K=10$ ). Because each run yields paired outcomes for the two pipelines (Original vs. Preprocessed) under identical conditions, we test the mean paired difference with a two-sided paired  $t$ -test ( $n=10$  runs). Normality of per-run differences is checked with the Shapiro-Wilk test; if violated, we report the Wilcoxon signed-rank test. Effect size is reported as Cohen's  $d$  for paired designs ( $d = \bar{d}/s_d$ ), where  $\bar{d}$  and  $s_d$  are the mean and standard deviation of the per-run differences. We test hypotheses as follows:

- **Null hypothesis ( $H_0$ ):**

No mean difference between conditions,

$$H_0 : \mu_{\text{orig}}^{(M)} = \mu_{\text{pre}}^{(M)}.$$

- **Alternative hypothesis ( $H_1$ ):**

A mean difference exists between conditions,

$$H_1 : \mu_{\text{orig}}^{(M)} \neq \mu_{\text{pre}}^{(M)}.$$

With TTA fixed at  $K=10$ , the preprocessed pipeline outperformed the Original pipeline by a modest yet consistent margin ( $\Delta\text{Acc} = +0.45$  pp).

Table 4 indicates a significant accuracy gain for the preprocessed pipeline with TTA. The column “Metric” indicates the score compared (here, Accuracy); “Diff. (pp)” is the average difference in percentage points between preprocessed and original (positive favors Preprocessed); “ $t$  (df)” is the paired  $t$ -test statistic with its degrees of freedom; “ $p$ ” is the probability of observing such a difference under the null (smaller means stronger evidence); and “Cohen's  $d$ ” is the standardized effect size (larger means a more consistent gain).

Table 4: Paired test at  $K=10$  (Original vs. Preprocessed).

Metric	Diff. (pp)	$t$ (df)	$p$	Cohen's $d$
Acc.	+0.45	5.72 (9)	<0.001	1.80

The results show that with TTA fixed at  $K=10$ , the preprocessed pipeline is, on average, +0.45 percentage points more accurate than the original pipeline. This improvement was consistent (Cohen's  $d = 1.80$ , large effect) and very unlikely to be due to chance ( $p < 0.001$ ).

With TTA, preprocessing helps and without TTA, the two pipelines perform essentially the same. In the no-TTA condition, the two pipelines were statistically

indistinguishable for Accuracy and F1 ( $p > 0.05$ ), reinforcing that preprocessing is beneficial primarily when paired with TTA.

#### 4.4 Addressing the Research Questions

The experiments in Sections 4.1 and 4.2 answer our research questions. Table 5 summarizes the findings.

Table 5: Summary of findings.

RQ	Finding
<b>RQ1</b>	<b>Preprocessing helps only when paired with TTA.</b> Without TTA, differences between the Original and Preprocessed pipelines were negligible; with TTA fixed at $K=10$ , the preprocessed pipeline showed a consistent, statistically significant gain (paired $t$ -test, $p < 0.001$ , $d = 1.80$ ).
<b>RQ2</b>	<b>TTA improves accuracy and stabilizes predictions.</b> TTA increases performance and reduces variability across runs; it also reveals and amplifies the subtle advantage of preprocessed inputs, acting as a key stabilizer under federated inference.

##### RQ1: Does preprocessing help or hinder classification?

Preprocessing helps classification only when TTA is applied. In the baseline federated setting without TTA (Section 4.1), the Original and Preprocessed pipelines performed comparably. With TTA at  $K=10$  (Section 4.2), the Preprocessed pipeline significantly outperformed the Original pipeline (paired  $t$ -test,  $p < 0.001$ ; see Table 4), indicating that the standardization benefits were realized at inference when augmented views were aggregated.

##### RQ2: To what extent does TTA improve robustness and accuracy?

TTA yields statistically significant improvements in accuracy and acts as a stabilization mechanism, reducing run-to-run variability and exposing systematic differences between training strategies (Section 4.2). In practice, TTA should be the default inference strategy; when the computational budget permits, pairing TTA with light preprocessing delivers additional reliable gains.

## 5 CONCLUSION

This study assessed the effects of standard preprocessing and TTA on federated MRI tumor classification. Using two clients, Original and Preprocessed, we compared pipelines under a fixed augmentation budget and quantified paired mean differences. Preprocessing alone has a negligible effect, whereas preprocessing combined with TTA yields consistent, statistically significant gains (e.g., +0.45 pp in accuracy;  $t(9) = 5.72$ ,  $p < 0.001$ ; Cohen’s  $d = 1.80$ ). In practice, TTA should be the default inference strategy; when the budget permits, pairing it with light preprocessing delivers additional reliable improvements.

In future work, we will scale to larger and more heterogeneous federations, adopt patient-level grouping when identifiers are available, and assess additional backbones (e.g., MobileNet, ResNet-34) to strengthen external validity. We will also broaden the augmentation policies and vary the number of TTA samples to map accuracy-cost trade-offs under non-IID conditions. These steps are essential to guide reliable, privacy-preserving AI for real-world clinical workflows.

## ACKNOWLEDGMENTS

The authors gratefully acknowledge the financial support of FAPEMIG (Grant #APQ00923-24). André R. Backes gratefully acknowledges the financial support of CNPq (Grant #302790/2024-1).

## REFERENCES

Albalawi, E., T.R., M., Thakur, A., Kumar, V. V., Gupta, M., Khan, S. B., and Almusharraf, A. (2024). Integrated approach of federated learning with transfer learning for classification and diagnosis of brain tumor. *BMC Medical Imaging*, 24:110.

Barbosa, G. V. G., Rodrigues, L. G. F., Rodrigues Moreira, L. F., and Backes, A. R. (2025). Federated learning in breast cancer diagnosis. *Revista de Informática Teórica e Aplicada*, 32(1):173–179.

Beutel, D. J., Topal, T., Mathur, A., Qiu, X., Fernandez-Marques, J., Gao, Y., Sani, L., Kwing, H. L., Parcollet, T., Gusmão, P. P. d., and Lane, N. D. (2020). Flower: A friendly federated learning research framework. *arXiv preprint arXiv:2007.14390*.

Carmo, N. C. d., Rodrigues Moreira, L. F., and Backes, A. R. (2025). Evaluating multiple combinations of models and encoders to enhance LDCT images. *Signal, Image and Video Processing*, 19(11):891.

Goodfellow, I., Bengio, Y., and Courville, A. (2016). *Deep Learning*. MIT Press. <http://www.deeplearningbook.org>.

He, K., Zhang, X., Ren, S., and Sun, J. (2016). Deep residual learning for image recognition. In *Proceedings of the IEEE Conference on Computer Vision and Pattern Recognition (CVPR)*, pages 770–778.

Islam, T., Hafiz, M. S., Jim, J. R., Kabir, M. M., and Mridha, M. (2024). A systematic review of deep learning data augmentation in medical imaging: Recent advances and future research directions. *Healthcare Analytics*, 5:100340.

Jiang, Y., Zhang, Y., Lin, X., Dong, J., Cheng, T., and Liang, J. (2022). Swinbts: A method for 3d multimodal brain tumor segmentation using swin transformer. *Brain Sciences*, 12(6):797.

Kaur, P. and Mahajan, P. (2025). Detection of brain tumors using a transfer learning-based optimized resnet152 model in mr images. *Computers in Biology and Medicine*, 188:109790.

Khaliki, M. and Başarslan, M. (2024). Brain tumor detection from images and comparison with transfer learning methods and 3-layer cnn. *Scientific Reports*, 14(1):2664.

Konečný, J., McMahan, H. B., Ramage, D., and Richtárik, P. (2016). Federated optimization: Distributed machine learning for on-device intelligence. *arXiv preprint arXiv:1610.02527*.

Louis, D. N., Perry, A., Reifenberger, G., von Deimling, A., Figarella-Branger, D., Cavenee, W. K., Ohgaki, H., Wiestler, O. D., Kleihues, P., and W., E. D. (2021). The 2021 who classification of tumors of the central nervous system: a summary. *Neuro-Oncology*, 23(8):1231–1251.

Mari, J., Rodrigues Moreira, L. F., Silva, L., Escarpinat, M., and Backes, A. (2025). Breast Cancer Image Classification Using Deep Learning and Test-Time Augmentation. In *Proceedings of the 20th International Joint Conference on Computer Vision, Imaging and Computer Graphics Theory and Applications - Volume 3: VISAPP*, pages 761–768. INSTICC, SciTePress.

McMahan, H. B., Moore, E., Ramage, D., Hampson, S., and Agüera y Arcas, B. (2017). Communication-efficient learning of deep networks from decentralized data. *Proceedings of the 20th International Conference on Artificial Intelligence and Statistics (AISTATS)*, 54:1273–1282.

National Institute of Standards and Technology (2012). Secure Hash Standard (SHS). Technical Report FIPS PUB 180-4, U.S. Department of Commerce.

Rodrigues, L. F., Naldi, M. C., and Mari, J. F. (2017). Exploiting Convolutional Neural Networks and Preprocessing Techniques for HEp-2 Cell Classification in Immunofluorescence Images. In *2017 30th SIBGRAPI Conference on Graphics, Patterns and Images (SIBGRAPI)*, pages 170–177.

Rodrigues, L. G. F., V. Gomes Barbosa, G., Moreira, R., Rodrigues Moreira, L. F., and Backes, A. R. (2025). Medical image classification with privacy: Centralized and federated learning comparison. *Revista de Informática Teórica e Aplicada*, 32(1):180–187.

Rodrigues Moreira, L. F., Moreira, R., Travençolo, B. A. N., and Backes, A. R. (2025). Deep learning based image classification for embedded devices: A systematic review. *Neurocomputing*, 623:129402.

Shah, H. A., Saeed, F., Yun, S., Park, J.-H., Paul, A., and Kang, J.-M. (2022). A robust approach for brain tumor detection in magnetic resonance images using finetuned efficientnet. *IEEE Access*, 10:65426–65438.

Shaikh, A., Amin, S., Zeb, M. A., Sulaiman, A., Al Reshan, M. S., and Alshahrani, H. (2025). Enhanced brain tumor detection and segmentation using densely connected convolutional networks with stacking ensemble learning. *Computers in Biology and Medicine*, 186:109703.

Siddique, N., Paheding, S., Elkin, C. P., and Devabhaktuni, V. (2022). Brain tumor detection and classification using machine learning: A comprehensive survey. *Visual Computing for Industry, Biomedicine, and Art*, 4(1):1–19.

Solanki, S., Singh, U. P., Chouhan, S. S., and Jain, S. (2023). Brain tumor detection and classification using intelligence techniques: An overview. *IEEE Access*, 11:12870–12886.

Stupp, R., Mason, W. P., van den Bent, M. J., Weller, M., Fisher, B., Taphoorn, M. J. B., Belanger, K., Brandes, A. A., Marosi, C., Bogdahn, U., Curschmann, J., Janzer, R., Ludwin, S., Gorlia, T., Allgeier, A., Lacombe, J.-P., Cairncross, J., Shaw, E., Jain, R. K., Mehta, M. J., Rampling, J. G. G., Wick, G. J., Wick, W., Westphal, M., Tonn, J. C., Mirimanoff, J. P., Eisenhauer, E., and Hegi, M. E. (2005). Radiotherapy plus concomitant and adjuvant temozolomide for glioblastoma. *New England Journal of Medicine*, 352(10):987–996.

Wang, G., Li, W., Aertsen, M., Deprest, J., Ourselin, S., and Vercauteren, T. (2019). Aleatoric uncertainty estimation with test-time augmentation for deep learning-based medical image segmentation. *Neurocomputing*. Wellcome/EPSRC Centre for Interventional and Surgical Sciences, UCL, KU Leuven.

Wen, P. Y. and Butler, M. (2020). Glioblastoma multiforme: biology and management. In *Abeloff's Clinical Oncology*, chapter 77. Elsevier, Philadelphia, 6 edition.

Zhou, L., Wang, M., and Zhou, N. (2024). Distributed federated learning-based deep learning model for privacy mri brain tumor detection. *arXiv preprint arXiv:2404.10026*.